Biochemistry

pubs.acs.org/biochemistry Article

Engineering of a Brighter Variant of the FusionRed Fluorescent Protein Using Lifetime Flow Cytometry and Structure-Guided Mutations

Srijit Mukherjee, Sheng-Ting Hung, Nancy Douglas, Premashis Manna, Connor Thomas, Annika Ekrem, Amy E. Palmer, and Ralph Jimenez*

Cite This: *Biochemistry* 2020, 59, 3669–3682 Read Online

ABSTRACT: The development of fluorescent proteins (FPs) has revolutionized biological imaging. FusionRed, a monomeric red FP (RFP), is known for its low cytotoxicity and correct localization of target fusion proteins in mammalian cells but is limited in application by low fluorescence brightness. We report a brighter variant of FusionRed, "FR-MQV," which exhibits an extended fluorescence lifetime (2.8 ns), enhanced quantum yield (0.53), higher extinction coefficient (~140 000 M^{-1} cm^{-1}), increased radiative rate constant, and reduced nonradiative rate constant with respect to its precursor. The properties of FR-MQV derive from three mutations—M42Q, C159V, and the previously identified L175M. A structure-guided approach was used to identify and mutate candidate residues around the para-hydroxyphenyl and the acylimine sites of the chromophore. The C159V mutation was identified via lifetime-based flow cytometry screening of a library in which multiple residues adjacent to the para-hydroxyphenyl site of the chromophore were mutated. The M42Q mutation is located near the acylimine moiety of the chromophore and was discovered using site-directed mutagenesis guided by X-ray crystal structures. FR-MQV exhibits a 3.4-fold higher molecular brightness and a 5-fold increase in the cellular brightness in HeLa cells [based on fluorescence-activated cell sorting (FACS)] compared to FusionRed. It also retains the low cytotoxicity and high-fidelity localization of FusionRed, as demonstrated through assays in mammalian cells. These properties make FR-MQV a promising template for further engineering into a new family of RFPs.

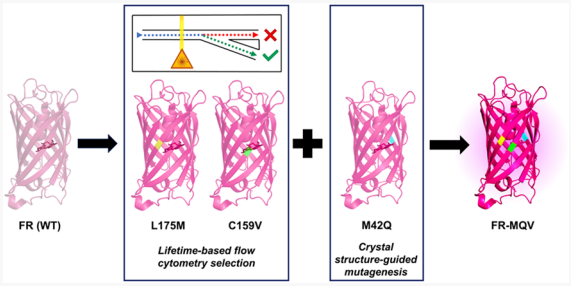

The availability of genetically encoded fluorophores such as fluorescent proteins (FPs) initiated a revolution in biological imaging.[1] Routine use of FPs in assays involving technologies, such as Förster resonance energy transfer (FRET),[2] fluorescence lifetime imaging microscopy (FLIM),[3,4] molecular sensing,[5] and nanoscopy,[6] makes them indispensable tools for biological research. Current efforts focus on developing FPs with excitation and emission in the far-red/near-infrared wavelengths and with photophysical properties such as photoswitching and fluorescence intermittency optimized for super-resolution imaging modalities.[7−10] Nevertheless, all imaging applications benefit from increased cellular brightness, which is strongly dependent on molecular brightness (defined as the product of the molar extinction coefficient and the fluorescence quantum yield).[11,12] Lifetime-based selection methods have exploited a correlation between fluorescence lifetime and quantum yield to develop FPs with higher quantum yield such as NowGFP,[13] mTurquoise2,[14] and mScarlet, which is the brightest red FP observed to date.[15]

FPs selected for higher fluorescence lifetime generally show a decreased rate constant of nonradiative decay (k_{nonrad}), ultimately resulting in increased quantum yield and higher brightness. However, quantum yield is also linearly related with k_{rad}; therefore, there is an interplay between the absorption probability and radiative emission probability. The Strickler−Berg equation formalizes the relationship between the k_{rad} and extinction coefficient, as well as other spectral properties such as the energies and profiles of the absorption and emission bands.[16] For example, blue shifts and decreased spectral width can lead to higher probabilities of radiative decay.[17] The relationship between spectral characteristics and the rate constants of energy decay have recently been discussed for FPs.[18,19] An engineering strategy that maximizes the radiative rate constant while simultaneously minimizing the nonradiative rate constant should be an effective way to brighten a FP.

These issues are particularly acute for red FPs (RFPs), which generally have lower values of fluorescence lifetime and

Received: June 8, 2020
Revised: September 4, 2020
Published: September 11, 2020

https://dx.doi.org/10.1021/acs.biochem.0c00484
Biochemistry 2020, 59, 3669−3682

quantum yield compared to shorter wavelength variants and are therefore not as bright.[20] The RFP chromophores contain an acylimine moiety, which expands their electronic conjugation and leads to a ∼50 nm red shift in their absorption and emission spectra with respect to green analogues like EGFP.[21,22] Many potential nonradiative decay mechanisms that lead to lower quantum efficiencies in such systems have been investigated, including transitions to dark states;[23,24] charge accumulation and twisting of the acylimine moiety;[25] changes in hydrogen bonding patterns; and electrostatic, steric, and conformational effects associated with their increased number of vibrational degrees of freedom.[26,27]

Cellular brightness depends on both photophysical and nonphotophysical factors such as translational efficiency, protein folding, and chromophore maturation.[28] FPs like FusionRed-M (FR-M) and mScarlet-I were developed to enhance cellular brightness over their brighter parents FR-1 and mScarlet, respectively.[15,29] Although there have been many efforts to improve the cellular and molecular brightness of FPs, performance in cell biology applications may still suffer from cellular toxicity, poor or overexpression in certain cellular contexts, and *in cellulo* oligomerization.[11,28] As discussed below, in the course of evaluating the performance of bright and commonly used RFPs, we found a trade-off between cellular brightness and localization fidelity of the GalT fusions of mScarlet, which led us to question whether the high cellular brightness associated with very high expression level leads to the appearance of mislocalized FPs.

FusionRed (FR) was developed as a noncytotoxic RFP that shows efficient and correct localization in multiple fusion constructs in different organisms.[30] However, this FP has not been widely adopted because it is relatively dim, in part due to its low quantum yield (0.19). We recently developed the FR-M variant (FR-L177M, numbered with respect to mCherry, and FR-L175M, numbered with respect to FR; see Supporting Information S1, Table S1), which is 1.9-fold brighter than FR in HeLa cells.[29] In this study, we used structure-guided engineering strategies to identify substitutions M42Q and C159V (sequence numbering with respect to FR) in the vicinity of the chromophore that individually increase the fluorescence lifetime of FR. These mutations led to the development of the bright triple mutant FR-MQV. We performed a detailed *in vitro* photophysical analysis which corroborated the increase in the molecular brightness in FR-MQV based on minimizing the k_{nonrad} and increasing the k_{rad}. Additionally, we investigated the cellular properties of FR-MQV and found that it is 5-fold brighter in HeLa cells [using fluorescence-activated cell sorting (FACS)] compared to the parent FR, while preserving its cellular properties such as low cytotoxicity and high-fidelity localization.

METHODS AND MATERIALS

Mutagenesis, Cloning, and Construct Development. *Yeast Constructs.* The QuickChange site-directed mutagenesis method was used for making point mutations using PfuTurboDNA polymerase and a thermocycler. Libraries with multiple site-directed targets were created using a splicing overlap extension reaction. Primers were designed to introduce the desired mutations, and the initial PCRs generate overlapping gene segments that are used as template DNA for another PCR to create a full-length product. Fresh competent yeast cells (*Saccharomyces cerevisiae* BY4741) were prepared prior to electroporation. Cells, DNA, and cut pYestDest52 vector were combined and left on ice for 5 min. Electroporation conditions (Bio-Rad Gene Pulser Xcell) were as follows: C = 25 μF, PC = 200 Ohm, V = 1.5 kV (in 0.2 cm cuvettes). Cells were passed twice prior to expression. Mutants were transferred to the pBad-His vector for expression/Ni-NTA protein purification.

Bacterial Expression Constructs. For bacterial expression, FR-Q and FR-MQ were made using the Q5 site-directed mutagenesis kit (New England Biolabs) with pBad-FR and pBad-FR-M, respectively, as the templates and the primers tCGCCACACAGGACACAAG and cCACATATGT-CTCATCGTCAGC. FR-MV was designed with similar protocols by inserting the C159V substitution into FR-M, with appropriate primers. FR-MQ C159V was also made via Q5 mutagenesis with the above primers and FR-M C159V as the template. The M42Q mutation was also made in pBad-mKate via Q5 mutagenesis, and the corresponding A44Q mutation was made in pBad-mScarlet and pBad-mCherry using overlap extension PCR.

Mammalian Expression Constructs for FACS. FR-MQ and FR-MQV were expressed as histone H2B fusion proteins in HeLa cells. Specifically, the FR-MQ and FR-MQV mutants were PCR amplified from the pBad constructs with the upstream primer GGTATGGCTAGCATGACTGGTG and a reverse primer that introduces a NotI site adjacent to the stop codon (acatGCGGCCGCTCATTTCCCTCCATC). Similarly, mScarlet-I (mScarlet T74I) was PCR amplified from a Q5-generated pBad construct (primers AGGGCCTTCA-tCAAGCACCCC and GCAGCCGTAC-ATGAACTGAGG) with the same upstream primer and a reverse primer that introduces an XcmI site adjacent to the stop codon. The FR-MQ and FR-MQV products were cut with *Bam*HI and NotI and ligated into *Bam*HI/NotI cut piggyBac-H2B, and the mScarlet-I product was cut with *Bam*HI and XcmI and ligated into *Bam*HI/XcmI cut piggyBac-H2B.

Mammalian Expression Constructs for OSER. To assess protein aggregation in mammalian cells, the mutants were expressed as fusions with CytERM in U2OS cells. FPs were amplified from the pBad construct with an upstream primer that introduces an AgeI site upstream of the start codon (gcatACCGGTCGCCACCATGGTGTCCG-AGCTGATTA-AGG) and the reverse primer described above that introduces a NotI site. The AgeI/NotI cut PCR product was ligated into AgeI/NotI cut CytERM vector and transfected into U2OS cells as described above for HeLa cells.

Mammalian Expression Constructs for GalT-FP Fusions. To localize our mutants to the Golgi, they were expressed as GalT fusions in U2OS cells. The *Bam*HI/NotI cut FR, FR-M, and FR-MQV PCR products described above were ligated into *Bam*HI/NotI cut GalT vector. mScarlet-I was cut from pBad with *Bam*HI and *Sal*I and ligated into *Bam*HI/*Sal*I cut GalT-mScarlet.

Microfluidic-Based Selection from Site-Directed Libraries. *Library Targets.* We targeted the positions 159, 161, 196, and 198 in FR (using FR numbering; Supporting Information S1), expressed the libraries in yeast (*Saccharomyces cerevisiae*), and screened this library on a lifetime flow cytometer.[29] Screening revealed the presence of brighter clones with longer and shorter lifetime than parent FR (lifetime ∼2.05 ns). We performed another two rounds of FACS enrichment on a BD FACSAria Fusion cell sorter to remove the dim/nonfluorescent clones. Position 159 was mutated to I, L, V, F, M, C, A, G, T, S, W, and R; position 161 to I, L, M, Q, N, H,

https://dx.doi.org/10.1021/acs.biochem.0c00484
Biochemistry 2020, 59, 3669−3682

and K; position 196 to I, V, A, and T; and position 198 to all possible amino acids. The library size was ∼7000 clones.

Post Microfluidic Sorting. After selection, the collected yeast cells were grown in liquid culture and then plated, and 25 clones with unique lifetimes were picked from these sorter-enriched libraries using a lifetime assisted plate-based screen discussed in a previous work.[29] The FR site-directed (FSD) clones with unique DNA sequences were further characterized (Supporting Information S2, Table S2).

Cell Growth, Transformation/Transfection, and Protein Purification Protocols. *Bacterial Transformation and Growth.* Bacteria (competent *E. coli*, Top10 strain) were transformed with the DNA encoding a FP of interest in the pBad-His vector. Roughly 2−5 μL of DNA (∼80 ng/mL concentrations) was slowly pipetted into ∼50 μL of competent cells (Invitrogen). The cells were left on ice for 20 min, heat shocked for 45 s at 42 °C, and then grown in antibiotic-free medium for 45 min. The cells were then plated (∼25−50 μL) onto ampicillin-containing LB agar plates and grown at 37 °C overnight. Colored colonies were picked from these plates and grown in 2XYT medium containing ampicillin overnight at 37 °C and 230 rpm. The next morning, 1 mL of this culture was added to 100 mL of fresh 2XYT with ampicillin and grown for 3 h at 37 °C to achieve an OD of ∼0.6, and then, 1 mL of 20% arabinose was added to the culture to initiate expression. The temperature of incubation was lowered to 28 °C to slow down bacterial growth and help protein folding and chromophore maturation. Depending on the maturation rate of the FP, they were grown at this temperature for 20−30 h.

Bacterial Cell Lysis and Protein Purification. The induced cell cultures were spun down at 8000 rpm for 20 min at 4 °C, and the cell pellet was frozen at −30 °C to ease lysis. Bacterial protein extraction reagent (B-PER, Thermofisher) was used to lyse the cells in the presence of protease inhibitor. The cells were lysed for 1 h at room temperature and then spun down at 11000 rpm and 4 °C for 15 and then 20 min to remove the cellular debris. The supernatant containing the 6x-His-tagged protein was filtered with a 0.45 μm polyethersulfone membrane syringe filter and incubated with Ni-NTA agarose for 1 h on ice. The resin was then loaded into a column and washed with 10 and 20 mM imidazole, and then, the proteins were eluted with 250 mM imidazole. The imidazole was removed using PD-10 desalting columns (GE HealthCare) or 24 h of dialysis using SnakeSkin dialysis tubing (ThermoFisher) into Tris-HCL buffer (pH 7.4) or saline PBS buffer. These samples were used for *in vitro* photophysical analyses.

Mammalian Cell Growth and Transfection. HeLa/U2OS cells were cultured in RPMI medium (Gibco Life Technologies) supplemented with penicillin/streptomycin (Gibco Life Technologies) and 10% heat-inactivated fetal bovine serum (Sigma-Aldrich) at 37 °C with 5% CO_2 plus humidity. For imaging experiments, U2OS cells were grown in 35 mm imaging dishes (made in-house from Corning 35 × 10 mm dishes with VWR 18 × 18 mm no. 1.5 coverslips). All CyTERM constructs were transiently transfected for 18−24 h using Lipofectamine 3000 (Invitrogen) or TransIT-LT1 transfection reagent (Mirus) according to the manufacturer's instructions. For FACS experiments, we used HeLa cells transiently transfected using the TransIT-LT1 reagent (Mirus, catalog no. MIR2304) and prepared for FACS analysis after 48 h.

***In Vitro* Photophysical Measurements.** *Instrumentation.* Absorption spectra were collected on a Cary5000 UV−vis near-IR spectrophotometer using a double beam mode with matched cuvettes and blank subtraction. Samples were diluted using 1X-Tris-HCl Buffer (pH ∼ 7.4), and absorbance was measured at optical densities (ODs) between 0.05 and −0.25 to maintain measurements in the linear range of Beer−Lambert's law. Fluorescence measurements were performed with a HORIBA Jobin Yvon Fluorolog-3 FL3-222 instrument.

Extinction Coefficient Measurements. Alkali denaturation was used to estimate the ratiometric values of the maximum extinction coefficient (EC_{max}) for the samples. The main text of the article reports an average of three or more independent measurements performed for FPs reported with a standard deviation error. FPs with fewer measurements are reported without an error bar. To measure the EC_{max}, the following protocol was used: (a) For Blank1, 900 μL of Tris-HCl buffer (pH 7.4) spectrum was recorded. (b) For Blank2, 900 μL of Tris-HCl buffer (pH 7.4) + 100 μL of 10 M NaOH (pH ∼ 14) was used. (c) 900 μL of Tris-HCl buffer (pH 7.4) + a few μL of concentrated pure protein sample was added to adjust the absorbance to a value of OD ∼ 0.1. A spectrum from 300−700 nm was recorded. (d) 100 μL of 10 M NaOH was added to this solution, and a spectrum in the same range was recorded immediately. Kinetic effects start playing a role on delaying the spectral measurement as degradation product peaks are known to drift in amplitude and wavelength over time.

Calculation of EC_{max}. We performed titration-based EC_{max} calculations for FR-M, FR-MQV, and mScarlet-I. The numbers obtained compare well to the values measured by the one-step alkali denaturing method.[11] The values were based on the mathematical relationship stated below, as FPs of the FR family are known to exhibit backbone cleavage.[30] To verify if this method was valid for FR-MQV, we also performed SDS-PAGE (Supporting Information S3a), where purified proteins (∼10 μg) were run on TruPAGE precast 4−20% gradient acrylamide gels (Sigma-Aldrich) in TEA−Tricine running buffer with the Spectra Multicolor Broad Range protein ladder (ThermoFisher). For other FPs that do not exhibit backbone cleavage, like mScarlet, the absorption at 380 nm was disregarded.

$$\epsilon_{\mathrm{maxRFP}} = \frac{\mathrm{Abs}_{\mathrm{maxRFP}}}{\left(\frac{\mathrm{Abs}_{380\mathrm{nm}}}{\epsilon_{380\mathrm{nm}}}\right) + \left(\frac{\mathrm{Abs}_{450\mathrm{nm}}}{\epsilon_{450\mathrm{nm}}}\right)}$$

Quantum Yield Measurements. Freshly prepared or flash frozen purified protein was diluted with Tris-HCl buffer (pH 7.4) in a 1 cm path length quartz cuvette to an OD of ∼0.1. A matched cuvette was used for baseline correction to measure absorption spectra. The same cuvette with the solution in it was transferred to the fluorimeter for collecting fluorescence spectra. After each absorption and emission scan, 200−250 μL of the sample was removed and replaced with fresh buffer to create a step dilution. This step dilution was repeated 4−5 times for each sample. RFPs were excited at 520 nm such that the entire emission spectrum was recorded for each FP (even for blue-shifted RFPs) with high enough absorption. For each FP, integrated fluorescence was calculated for the area under the RFP emission feature on the emission spectra and was plotted against the corresponding OD at 520 nm from the absorption spectrum. The integrated fluorescence versus OD plot can be fitted with a straight line (Supporting Information S3b) of the form y = slope × x, where y is the integrated fluorescence, and x is the OD.

https://dx.doi.org/10.1021/acs.biochem.0c00484
Biochemistry 2020, 59, 3669−3682

$$\text{quantum yield}_{\text{sample}} = \text{quantum yield}_{\text{ref}} \times \text{slope}_{\text{sample}} \times n_{\text{sample}}{}^2/\text{slope}_{\text{ref}} \times n_{\text{ref}}{}^2$$

where the refractive index of the sample and the reference are n_{sample} and n_{ref}, respectively. mCherry (quantum yield = 0.22 in Tris-HCl, pH 7.4), Cresyl Violet (quantum yield = 0.54 in EtOH), and mScarlet (quantum yield = 0.72 with respect to mCherry) were used as references.[11,15]

pK_a Measurements. pK_a measurements were performed by preparing buffers in the range of pH 2−12. The pH was measured for each buffer to confirm the calculated pH values using a pH meter. Fixed amounts of concentrated pure protein samples were added to 1 mL of buffer in a quartz cuvette with a 1 cm path length, and a fluorescence spectrum was recorded in each case with excitation at 520 nm. The maximum value of fluorescence counts was used to normalize the fluorescence spectra for each protein. The data were plotted and fitted to the sigmoidal curve shown (Supporting Information S4a). The calculated pK_a values and reported values for published RFPs have been provided in the Supporting Information S4a, Table S4. Buffers in the pH range 2−3 were prepared with a dilution of glycine and 1 M HCl. Those in the range 3−6 were prepared using dilutions of 0.1 M citric acid and 0.1 M Na-citrate, those in the range 6−8 with dilutions of 0.2 M Na_2HPO_4 and 0.2 M KH_2PO_4; and those in the range of 9−12 with dilutions of 0.2 M glycine and 1 M NaOH, and Tris-HCl buffer was used for the pH 7.4 measurement.

Fluorescence Lifetime Measurements in the Lifetime Flow Cytometer. The lifetime flow cytometer utilizes frequency-domain phase fluorimetry to select analytes based on excited state lifetime. The details of this setup are discussed in our previous publications.[29,31] The excitation beam is sinusoidally modulated at 29.5 MHz. The observed fluorescence signal is modulated at the same frequency as the excitation beam, but has a lower modulation depth and a phase shift that corresponds to the average time spent by the analyte in the excited state (average lifetime). A high-speed lock-in amplifier determines the phase shift, which is then converted to a lifetime value in the time domain.

$$\text{lifetime}_{\text{analyte}} = \text{lifetime}_{\text{reference}}(\text{ns}) + \text{tangent}(\text{phase-shift})/29.5\ \text{MHz}$$

For the reference, mCherry (∼1.6 ns) was used. FR had a mean lifetime 2.05 ± 0.15 ns on this device.

Steady-State Lifetime Measurements for Pure Proteins and Lysates. All lifetime measurements on purified proteins or filtered cell lysates were performed on a commercial TCSPC system (Fluoro-time 100, PicoQuant) using a 560 nm pulsed laser diode head excitation source with a repetition rate of 5 MHz. Emission was collected using either a red filter set (600 ± 30 nm) or a far-red filter set (670 ± 30 nm), to check for multiple species in the excited state or interconverting forms. The instrument response function (IRF) was collected using Ludox (Millipore Sigma) colloidal silica, whereas the samples were diluted to an OD value <0.05 for the measurement. A minimum of 20 000 photon counts were used to generate the fluorescence decays. The fluorescence transient decays were fitted to an iterative reconvolution with a biexponential function (or triexponential depending on the protein). The amplitudes and the components of the fits are provided in the Supporting Information S4b.

Photobleaching Measurements. Photobleaching measurements were performed using an LED excitation source (Lumencor) on an Olympus IX-73 fluorescence microscope with *E. coli* cells expressing the FP of interest. Bacteria on plates were washed and dispersed in aqueous blank buffer containing 0.17% (w/v) yeast nitrogen base (Sigma-Aldrich) and 0.5% (w/v) ammonium sulfate (Sigma-Aldrich) and then photobleached with excitation rate-normalized LED light. To bleach the sample, a 560 nm LED was used, whereas for repopulation with blue light, a 438 nm LED light source was used. Details of the measurements are discussed in the Supporting Information S4c.

Brightness in E. coli. To assess the cellular performance of the FR clones in this study, we performed a bacterial brightness assay at the single cell level on a droplet microfluidic sorting platform.[31] Two biological replicates with three independent technical triplicates were performed for each measurement. The bacteria were grown, and expression was induced as previously described; cytometry was carried out at ∼20−22 h after starting induction. Each technical replicate involved 10000 cells. Details of the screening protocol have been discussed in the Supporting Information S4d and a previous publication.[31]

Cellular Brightness Assays. *Brightness in HeLa Cells.* (a) For flow cytometry, the proteins of interest in the FR family, along with some standard RFPs including mScarlet, mScarlet-I, and mCherry, were fused to histone H2B and expressed in HeLa cells. Single-cell brightness was assessed by selecting single healthy cells based on forward and side-scattering photon counts on a BD FACSCelesta single cell analyzer after 48 h of transfection. Untransfected cells were used as a control to background subtract and analyze the fluorescence in the red and green channels for the proteins of interest. In most cases (except mScarlet-I with only one biological replicate), three or more biological replicates with three technical replicates of each were analyzed to determine the mean fluorescence with standard deviation based on the number of measurements (Supporting Information S5a). The samples were excited by a 561 nm laser line for collecting red fluorescence through the TRITC filter set (585/30 nm) and a 488 nm laser line for collecting through a GFP filter set (530/30 nm). The residual fluorescence from the green channel was effectively at the background level of the EGFP-H2B control (displaying signal values ∼20-fold higher than mScarlet with the highest green fluorescence in the series). Brighter red mutants had a higher green fluorescence background, suggesting red fluorescence bleeding through the green channel. (b) For confocal microscopy, HeLa cells grown in 35 mm imaging dishes (made in-house from Corning 35 × 10 mm dishes with VWR 18 × 18 mm no. 1.5 coverslips) were imaged 48 h post-transfection to maintain consistency with the FACS measurements. Before imaging, cells were washed three times with 2 mL of phosphate-free HEPES-buffered Hanks' balanced salt solution (HHBSS) containing 20 mM HEPES (Sigma), pH 7.4 and resuspended in 1.5 mL of the same buffer. Imaging was performed on a Nikon Ti-E spinning disc confocal microscope system. The imaging dishes were mounted on the microscope in an environmentally controlled chamber (Oko Laboratories; set to 37 °C, 5% CO_2, 90% humidity) and viewed with a 40× (numerical aperture, NA 0.95) air objective. A 560 nm laser was used for illumination, and a 590−650 nm band-pass filter (TRITC) was used for the detection of fluorescence with 200 ms exposure time and 20% laser power of the instrument. To minimize photobleaching, the focus of the microscope was adjusted to a lower laser power (5%) at only the center spot of the large image. Prolonged exposure of FR and its mutants to

https://dx.doi.org/10.1021/acs.biochem.0c00484
Biochemistry 2020, 59, 3669−3682

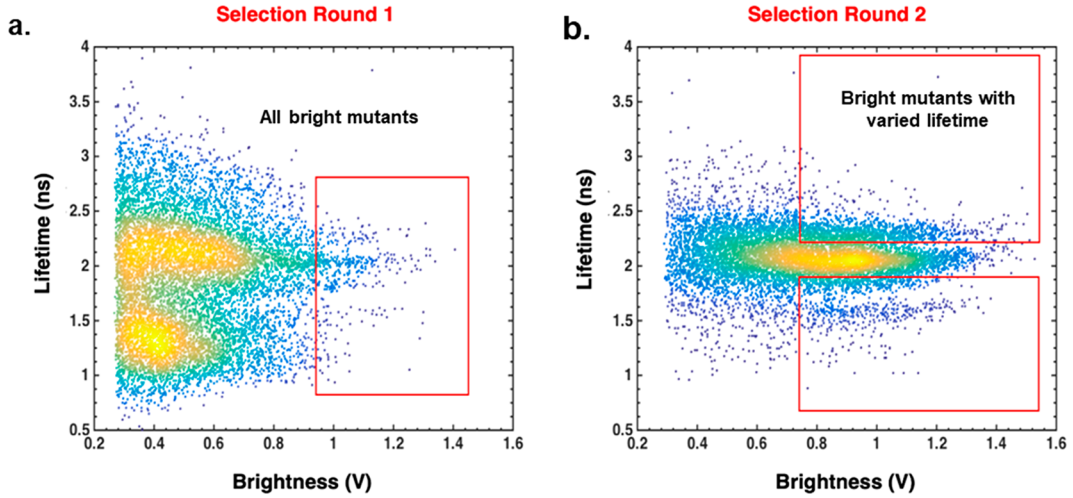

Figure 1. Fluorescence lifetime (vertical axis) vs brightness (horizontal axis) screening dot-plots of the FR site-directed library targeting sites near the para-hydroxyphenyl moiety, after two rounds of fluorescence-activated cell sorting (FACS) enrichments. Pseudocoloring represents normalized cell counts, where yellow indicates a higher cell count, and blue indicates a lower cell count. Red boxes indicate the selection gates for multiparameter microfluidic sorts. (a) First round of sorting for selecting bright clones. (b) The second round of sorting was performed in two batches using sorting gates for high brightness with different lifetime ranges. The mean fluorescence lifetime of FR measured on this instrument was 2.05 ns.

laser light can lead to lower brightness, which was a critical factor for this assay. Large images (~1600 × 1000 μm) were taken for each dish for each replicate. Details for this assay are presented in Figure 4b and the Supporting Information S5a.

Data Analysis for Brightness Assays Using Confocal Microscopy. The imaged cells were analyzed using the suite CellProfiler.[32] A pipeline was created that would identify objects that are above the noise background. A binarized image was thus created, and then, a gate to filter object typical of the size of nuclei was selected (2−25 μm), which selected the fluorescing nuclei in the H2B construct. The filtered objects in the parent cells were then quantified for mean brightness. Untransfected cells with cellular autofluorescence were the first to be analyzed, which gave us the estimation of bleed-through fluorescence.

Cellular Localization Assays. *Imaging Conditions.* U2OS cells were transfected with the constructs of interest as described previously. The cells were imaged 24 h post-transfection with a Nikon Ti-E spinning disc confocal microscope. Several large images (~1680 × 1000 μm) were captured while scanning the *z*-focus (*z*-stacks) for optimum focusing of all the cells appearing in the field of view. The typical scanned depth was 5.0−7.8 μm and was evenly separated into 5−7 layers. Maximum intensity projection of the *z*-stacks was used for the quantification of the OSER score. For GalT scoring, *Z*-stacks and independent frames were used for quantification of localization of FPs to the Golgi.

Data Analysis. The data analysis for the quantification of OSER scores was done in accordance with our previous report.[29] In brief, the suite CellProfiler was used to develop a pipeline that can identify cells based on size (20−50 μm), shape, and fluorescence intensity. The program identifies oligomerization substructures in these cells, filters them, and then quantifies them as whorls. The pipeline further continues to relate the number of whorl structures with each cell, and a MATLAB code quantifies the number of perfect and imperfect (cells with whorls). A score of 100 indicates that 100% of the cells are whorl-free, and 0% indicates that all cells have whorls in them. FR and its mutants display a high OSER score, whereas TagRFP-T was used as a negative control. The imaging data for the GalT-FP construct were analyzed using a blinding approach where multiple individuals were provided with image sets that were randomized. Individual images were scored as having fluorescence signal localized to the Golgi (characterized by a fistlike structure near the nucleus) or not. The approximate size of a healthy nucleus was estimated using ImageJ.[33] If the cells expressed FP outside this fistlike structure in the form of puncta or just smeared across the cytoplasm, they were considered mislocalized.

Chromophore Maturation Kinetics and Cytotoxicity. *Cytotoxicity Assay.* HeLa cells were transfected with the H2B-FP fusion constructs as discussed previously. Two biological replicates were prepared for each FP. Day 2 was defined as 48 h post-transfection. RFP and EGFP transfected cells were mixed at a 50:50 ratio by volume. A sample of the cell mixture was prepared for a flow cytometry measurement (BD FACSCelesta) to determine the actual RFP:EGFP ratio. The rest of the mixture was replated for further growth and proliferation. Independent screens of just EGFP cells and RFP cells were carried out first. Cells with green fluorescence higher than background were classified as "EGFP", and cells with red fluorescence higher than background were classified as "RFP". On day 6, the replated cells were again subjected to flow cytometry to quantify the change in the RFP and EGFP populations and determine a relative level of cytotoxicity. The cytotoxicity score was then calculated as the change in the RFP:GFP ratio for each sample. EGFP was used for normalization because it has been shown to be minimally cytotoxic.[34] The data for the assay are presented in the Supporting Information S5b.

Maturation Kinetics. Bacteria (top 10, *E. coli*) expressing FPs were grown in expression media for 4 h (28 °C, 230 rpm) to facilitate FP production in the exponential growth log phase. Chloramphenicol (250 μg/mL) was added to the cultures to stall bacterial growth and protein production.[35] The cultures were maintained at 37 °C and 230 rpm, and aliquots were taken every 30−60 min to measure the optical density (OD) and fluorescence. The $t_{1/2}$ at 37 °C was calculated by

https://dx.doi.org/10.1021/acs.biochem.0c00484
Biochemistry 2020, 59, 3669−3682

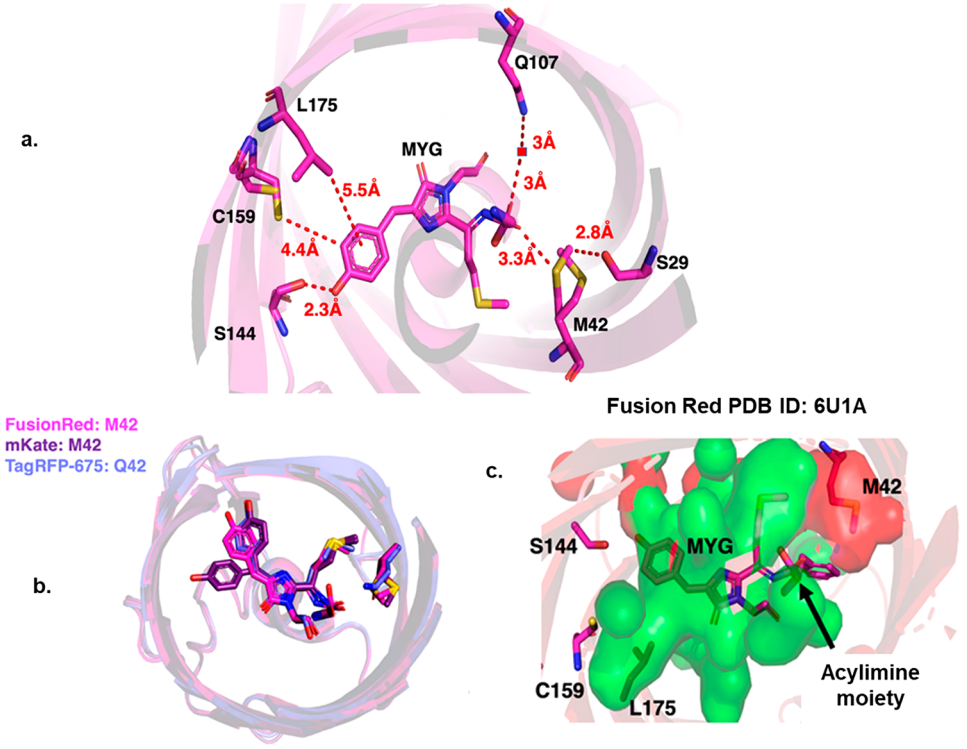

Figure 2. (a) Crystal structure of FR with positions around the chromophore relevant to the study generated using PyMol. (b) Comparative locations of the 42 position in TagRFP-675 (PDB ID, 4KGE; blue, 42Q), mKate (PDB ID, 3BXB; purple, 42M), and FR (PDB ID: 6U1A; pink, 42M). The crystal structure of mKate (PDB ID, 3BXB) indicates that the end of the chromophore near the para-hydroxyphenyl moiety may exist in both cis and trans conformations, with the cis conformer overlapping with that of TagRFP-675. For FR, the fluorescent chromophore exists in the cis conformation as well. (c) The occupancy surfaces (based on PyMol) indicate that the chromophore (green surface) and the side chain of the M42 residue (red surface) come in close contact.

Table 1. Summary of *in Vitro* Photophysical Properties of FR Mutants Developed in This Study vs Remeasured Values for Some Well-Characterized RFPs[a]

FP	λ_{abs} (nm)	λ_{em} (nm)	LT (ns)	QY	EC_{max} (M^{-1} cm^{-1})	molecular brightness	k_{rad} (μs^{-1})	k_{NR} (μs^{-1})
FR	574	596	1.78 ± 0.04	0.24 ± 0.04	94 000 ± 7000	1	135 ± 23	427 ± 26
FR-M	571	591	2.13 ± 0.05	0.34 ± 0.02	78 000 ± 10 000	1.2	160 ± 10	310 ± 15
FR-Q	568	587	2.10 ± 0.05	0.33 ± 0.01	133 000 ± 2000	2	157 ± 6	319 ± 13
FR-V	573	594	1.96 ± 0.02	0.31 ± 0.04	84 500 ± 8000	1.2	154 ± 4	361 ± 9
FR-MV	569	592	2.39 ± 0.02	0.38 ± 0.09	85 000 ± 6500	1.4	166 ± 5	254 ± 9
FR-MI	575	595	1.75 ± 0.02	0.26 ± 0.04	82 000	1	149 ± 12	423 ± 13
FR-MQ	567	586	2.43 ± 0.08	0.43 ± 0.08	130 000 ± 9000	2.7	176 ± 14	233 ± 19
FR-MQV	566	585	2.77 ± 0.07	0.53 ± 0.03	144 000 ± 3000	3.4	191 ± 12	170 ± 16
mScarlet-I	570	591	3.26 ± 0.07	0.59 ± 0.03	102 500 ± 4500	2.7	184 ± 10	128 ± 12
mKate	588	634	2.26 ± 0.07	0.33	48 000	0.7	130	264
mKate-M42Q	577	654	2.16 ± 0.05	0.17	25 000	0.2	79	384
mCherry	586	607	1.67 ± 0.07	0.22 (ref)	75 000 ± 5000	0.8	137	488
mScarlet	569	592	3.87 ± 0.07	0.71 (ref)	103 000 ± 4500	3.3	186	72

[a]The standard deviation error has been reported for measurements where independent triplicates were performed. mCherry and mScarlet were used as references for the quantum yield measurements.[11,15]

calculating the time required for the FP to reach half the maximum fluorescence value. The data for the assay are presented in the Supporting Information S5c.

RESULTS

Lifetime-Based Selection of a Site-Directed Library near the para-Hydroxyphenyl Moiety of the Chromophore Identifies the C159V Mutation. Four positions near the para-hydroxyphenyl moiety of the chromophore—C159, M161, V196, and H198—were simultaneously mutated in FR to generate a ∼7000-member library (see the Methods and Materials section for details of library generation). We employed lifetime-based microfluidic flow cytometry[29] to select variants with increased brightness and values of fluorescence lifetime different from the parent (Figure 1). Sequencing of selected clones revealed that H198 and V196 were conserved, but positions 159 and 161 showed sequence diversity (Supporting Information S2, Table S2). Furthermore, the selected population contained two clones, FR-C159V and FR-C159L, with higher cellular brightness than the parent FR,

https://dx.doi.org/10.1021/acs.biochem.0c00484
Biochemistry 2020, 59, 3669−3682

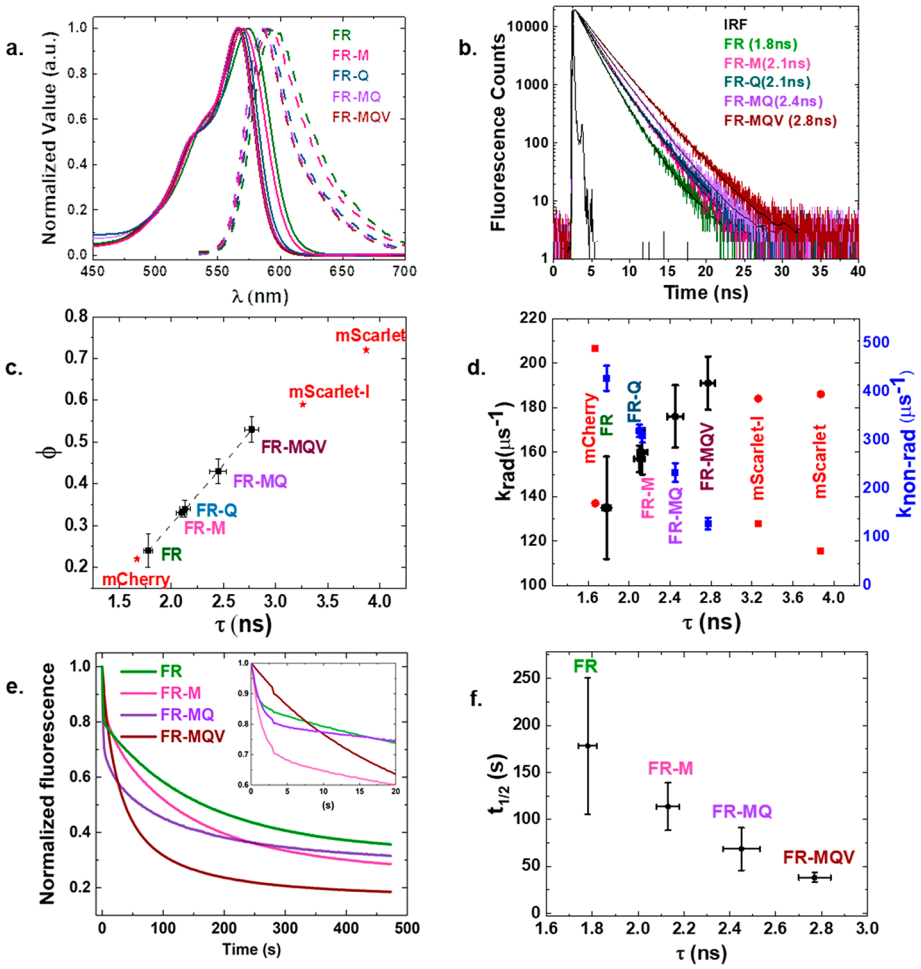

Photophysical analysis of the FR family of proteins

Figure 3. Photophysical properties of the FR family of FPs. (a) Absorption (solid lines) and emission (dashed lines) spectra. (b) TCSPC lifetime traces. Longer decay profiles indicate the gradual increase in fluorescence lifetime. The black lines indicate exponential fitting for the decay profiles. (See the Supporting Information S4b for fitting details.) (c) Plot of quantum yield versus fluorescence lifetime. The dashed line indicates the linear rise of quantum yield with increments in fluorescence lifetime for the FR family of FPs. The values for mCherry, mScarlet, and mScarlet-I are taken from refs 11 and 15. (d) Plot showing the increase in radiative rate constant (black) and decrease in nonradiative rate constant (blue) across the FR family relative to mCherry and mScarlet (red). Vertical error bars (blue and black) in the FR family indicate the uncertainty in the calculated rate constants; the horizontal error bars (black) are the standard deviation error in the measurement of fluorescence lifetime. (e) Photobleaching traces for the family of FR mutants, determined by averaging ∼10 decay traces in *E. coli* cells for each FP under normalized excitation rates. (f) Dependence of the fluorescence decay half-life on the excited state lifetime. Error bars indicate standard deviation errors.

but with differing lifetimes. FR-C159V had an increased lifetime of 2.0 ns, whereas FR-C159L had a decreased lifetime of 1.2 ns (cf. 1.8 ns lifetime for FR: details in the Supporting Information S2, Table S2). Of the two clones, FR-C159V was selected for further development in combination with the mutations identified below because it had the longer lifetime and because it did not show the complex photoactivation behavior seen in FR-C159L (Supporting Information S4c, Figure S4a).

The M42Q Mutation Adjacent to the Acylimine Moiety of FR Increases the Extinction Coefficient, Quantum Yield, and Fluorescence Lifetime. Mutations that alter the hydrogen-bonding structure surrounding and interacting with the acylimine moiety of the chromophore produce RFPs with extended Stokes shifts.[36−39] In addition to the site-directed library aimed at mutating the end of the chromophore near the para-hydroxyphenyl moiety, we investigated the end of the chromophore near the acylimine moiety in the crystal structures of mKate (PDB ID: 3BXB), the far-red emitting FP TagRFP-675 (PDB ID: 4KGE), and FR (PDB ID: 6U1A) using PyMol[40] (Figure 2 and Supporting Information S6). Based on the structural similarity, conformational freedom, and the fact that the side chain at position 42 is a known hot-spot for altering the hydrogen-bonded chemistry in mKate and TagRFP-675,[38] we incorporated a single point mutation M42Q into FR. The FR-M42Q (or FR-Q) mutant shows a 41% increase in the maximum extinction coefficient, an 18% increase in fluorescence lifetime, and a 42% increase in quantum yield (Table 1 and Figure 3). The mutation also resulted in blue-shifted and narrower absorption and emission spectra and a minor change in Stokes shift (Figure 3a and Supporting Information S4e−g). These properties reflect the higher radiative rate constant calculated for this mutant in comparison to FR (Figure 3d). Consequently, we performed site-saturation mutagenesis (library size = 20) at this position in the context of FR-M and found that the parent along with FR-M M42Q (FR-MQ) and FR-M M42I (FR-MI) were the only variants with observable red fluorescence. FR-MQ was the

https://dx.doi.org/10.1021/acs.biochem.0c00484
Biochemistry 2020, 59, 3669−3682

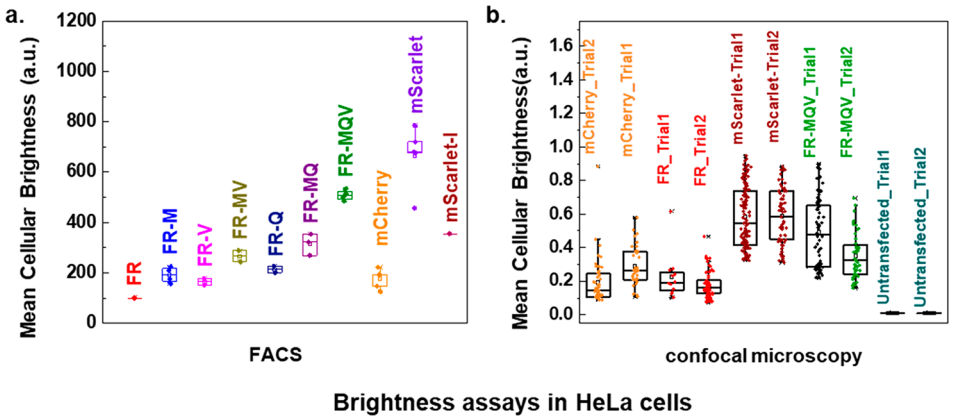

Figure 4. (a) FACS-based brightness assays of FPs expressed as histone H2B fusions in HeLa cells. Each biological replicate involved three technical replicate screens of ~10 000 individual cells. (b) Mean brightness values of individual HeLa cells obtained from confocal microscopy for histone H2B fusions. Each dish was an independent biological replicate and contained ~100 cells. For both parts a and b, the cells were sampled ~48 h post-transfection. Details of the assays are provided in the Supporting Information S5a. Error bars indicate standard deviation errors.

brightest species with a quantum yield of ~43% and a further increase of fluorescence lifetime by 0.3 ns. FR-MI showed decreases in maximum extinction coefficient, quantum yield, and fluorescence lifetime; thus, we did not pursue engineering of this variant. We investigated the effects of analogous mutations on closely related RFPs and noted rather different outcomes. For example, mKate M42Q shows a decrease in the molecular brightness due to ~50% decreases in both maximum extinction coefficient and quantum yield, along with a blue-shifted absorption spectrum and a significantly increased Stokes shift, all of which are consistent with previous findings.[38,39] In addition, analogous mutations at position A44 on mCherry and mScarlet-I RFPs resulted in non-fluorescent clones. It should be noted that mCherry, mScarlet-I, and FR show multiple structural differences in the chromophore structure and in the vicinity of the chromophore. Although crystal structures indicate that there seems to be sufficient space to accommodate a 44Q side chain in mCherry and mScarlet-I, there are multiple structural differences between the three FPs. We cannot explain why this mutation did not produce a fluorescent species in mCherry and mScarlet-I.

While measuring the maximum extinction coefficient with the alkali-denaturation method, we observed that M42Q containing mutants of FR produce a single hydrolysis product with an absorption band centered at 380 nm (Supporting Information S4h). Most RFPs, such as mScarlet, mCherry, and mRuby3, display GFP-like degradation with an absorption band at 450 nm. The hydrolysis products of FR variants with the native 42 M have both 380 and 450 nm absorption peaks. The 380 nm band is assigned to the cleavage of the chromophore from the β-carbon of the Tyr moiety in the chromophore.[41,42] The absence of the 450 nm band in FR-Q and FR-MQ reveals an alteration of the chromophore hydrolysis chemistry. This suggests that the 42Q residue interacts strongly with the chromophore in FR.

Combining Mutations M42Q, C159V, and L175M Led to the Generation of Bright FR-MQV. Each individual mutation results in an increment of fluorescence lifetime by ~0.3 ns in FR. Therefore, we incorporated all three mutations into FR to yield FR-MQV. The FR-MQV mutant exhibits a fluorescence lifetime of 2.8 ns which results in a high quantum yield of 53% (Figure 3b,c). The absorption and emission spectra are similar, with a slight blue shift and narrowing of the spectra in all variants possessing the M42Q mutation (Figure 3a and Supporting Information S4f,g). The molecular brightness of FR-MQV is ~3.4-fold higher than that of FR. Overall, we see increases in fluorescence lifetime and quantum yield, as a result of an increase in the radiative rate constant and a concomitant decrease in the nonradiative rate constant (Figure 3d). Steady-state absorbance and fluorescence spectra along with wavelength-dependent lifetime measurements were collected to assess the heterogeneity of chromophore formation. We found that FR-MQV matures predominantly into a red-emitting chromophore which emits as a single red-emissive species (Supporting Information S4b,i,j). FR-MQV has a low *in vitro* pK_a of ~4.6, like other members of the FR family (Supporting Information S4a) and breaks down into a single product of alkali hydrolysis, resembling FR-Q and FR-MQ (Supporting Information S4h). We also found that FR-MQV was ~2-fold brighter than FR in *E. coli* (Supporting Information S4d).

The photobleaching traces of FR-MQV and related variants are shown in Figure 3e. When photobleaching measurements were performed on multiple FPs illuminated at the same excitation rate, longer fluorescence lifetime is correlated with faster photobleaching (Figure 3f). In this case, excitation rates are set by ensuring that the value of excitation power (P, in mW) from the objective divided by the absorption cross section at 560 nm P/σ_{560nm} (defined as $\sigma_{560nm} = 2303 \times EC_{560}/N_A$; where EC_{560} is the extinction coefficient at 560 nm, and N_A is the Avogadro constant) is the same for the FPs being compared. Furthermore, it was observed that, under continuous irradiance of ~5 W/cm^2 at 560 nm, the fluorescence kinetics of FR variants with a C159 residue show two decay time scales. This behavior is typical of most FPs, which show an initial decay due to dark state conversion (also sometimes called reversible photobleaching), along with a slower time scale of permanent photobleaching.[43,44] The C159V and C159L mutations, which incorporate aliphatic groups, significantly reduce the amplitude of the faster decay component (Supporting Information S4c, Figure S4a). To verify that the faster component corresponds to a reversible process, we used alternating pulses of 560 and 438 nm excitation (Supporting Information S4c). The FR-C159V variant showed little recovery, and FR-C159L showed slight

https://dx.doi.org/10.1021/acs.biochem.0c00484
Biochemistry 2020, 59, 3669−3682

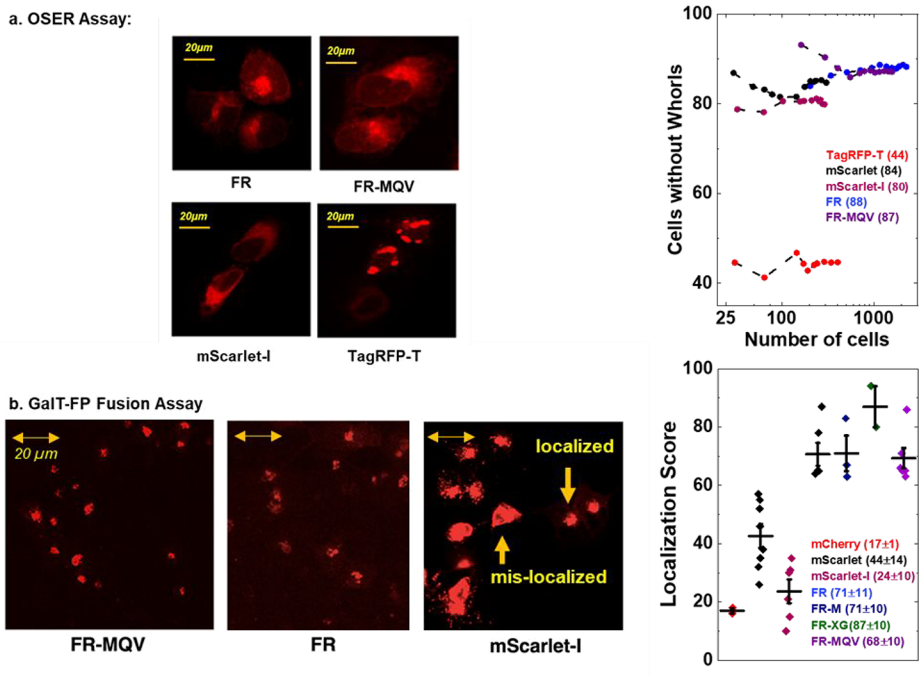

Figure 5. (a) OSER assay: representative maximum intensity projected confocal images for U2OS cells expressing cytERM-FP constructs for FR, FR-MQV, mScarlet-I, and TagRFP-T (negative control), and the graphical representation of the OSER scores for these cells. The *y*-axis on the plot indicates the percent cells that do not express subcellular "whorls". The OSER scores for this assay were as follows: FR, 88 (2250 cells); FR-MQV, 87 (1580 cells); mScarlet, 84 (306 cells); mScarlet-I, 80 (291 cells); and TagRFP-T, 45 (406 cells). (b) GalT-FP fusion assay: confocal microscope images for U2OS cells expressing the GalT-FP fusion constructs for FR-MQV, FR, and mScarlet-I, with the localization scores (indicative of the percent cells with the FP localized correctly to the Golgi) plotted for each RFP. The microscopy images show cells expressing GalT-mScarlet localized and mislocalized to the Golgi. The scores for FPs analyzed in the study have been reported with the FR mutants (including previously published FR-XG[29]) outscoring mCherry and mScarlet. Error bars indicate standard deviation errors across biological replicates.

recovery of the fluorescence; however, the recovery was much larger for FR (~20% higher). These results show that the reversible photobleaching dynamics of FR are influenced by the chemical nature of the side chain at position 159.

FR-MQV is 5-Fold Brighter in HeLa Cells and Retains the Cellular Properties and High-Fidelity Localization of FR. Flow cytometry and confocal microscopy were employed to quantify the cellular brightness of FR-MQV in HeLa cells (Figure 4). FACS screening of HeLa cells expressing FPs fused to histone H2B protein after 48 h of transfection revealed that FR-MQV is 5-fold brighter than the parent FR and ~1.4-fold less bright than mScarlet (Figure 4a and Supporting Information S5a). Measurements with confocal microscopy on the same construct revealed that FR-MQV is ~2.3-fold brighter than FR and ~1.4-fold dimmer than mScarlet (Figure 4b and Supporting Information S5a). We next investigated whether the mutations in FR-MQV would influence cytotoxicity, chromophore maturation, and localization of fusion proteins. FR-MQV exhibited low cytotoxicity, like the parent FR and in contrast to mCherry, which showed a ~80% relative decrease in cells expressing the FP after 6 days of expression (details of the assay are discussed in the Supporting Information S5b). FR-MQV showed chromophore maturation kinetics identical to the parent FR ($t_{1/2}$ ~ 195 min at 37 °C; Supporting Information S5c) and similar to mScarlet ($t_{1/2}$ ~ 130 min at 37 °C), but slower than mScarlet-I ($t_{1/2}$ ~ 45 min at 37 °C).

Overexpression and oligomerization in cells can lead to unwanted effects such as self-quenching, misfolding, mislocalization, and disruption of organelle structure and function.[45,46] Hence, we performed the organized smooth endoplasmic reticulum assay (OSER) assay[47] and examined localization of a GalT-FP fusion to assess the *in cellulo* monomericity and localization properties of FR-MQV relative to FR and the other bright RFPs mScarlet and mScarlet-I.

In the OSER assay, FPs are fused to the cytoplasmic end of the endoplasmic reticular signal anchor protein (cytERM).[47] Membrane localization increases the local concentration leading to the formation of dimers or higher-order oligomers that distort the ER structure which are observed as cellular substructures or "whorls". Figure 5a shows confocal microscopy images of cytERM-FPs expressed in U2OS cells and the corresponding OSER scores. TagRFP-T (positive control) shows characteristic oligomerization in the form of subcellular "whorls", while the FR mutants, mScarlet and mScarlet-I, generally lack such structures (see the Methods and Materials section for details of experiments and data analysis). In this work, we measured a score of 88 for FR and 87 for FR-MQV which are ~5% higher than that measured for mScarlet (84) and ~10% higher than that for mScarlet-I (80). We also developed GalT-FP fusions to localize the FPs of interest to the Golgi. Proper localization and mislocalization to the Golgi in U2OS cells imaged using confocal microscopy are shown in Figure 5b. Our analysis indicates that FR-MQV and other FR-derived mutants outscore mScarlet and mCherry in terms of proper localization to the Golgi. Our results are qualitatively consistent with previous observations where FR correctly localizes to the Golgi, but GalT-mCherry frequently displays puncta in the cytoplasm.[48] We observed higher occurrences of mislocalization in the bright RFPs mScarlet and mScarlet-I

https://dx.doi.org/10.1021/acs.biochem.0c00484
Biochemistry 2020, 59, 3669−3682

Table 2. Molecular Brightness of FR-MQV Is ~3-Fold That of FR, while FACS Measurements Indicate That It Is ~5-Fold Brighter In HeLa Cells[a]

protein	molecular brightness (EC_{max} × QY)	bacterial cell brightness (585 ± 15 nm)	HeLa cell brightness (585 ± 15 nm)	normalized relative to FR-M: molecular brightness	normalized relative to FR-M: HeLa cell brightness
FR	1	1	1	0.9	0.5
FR-M	1.2	1.3	2.1	1	1
FR-Q	2	1.4		1.7	
FR-MQ	2.6	1.7	3.6	2.3	1.7
FR-MQV	3.4	1.9	5.3	2.9	2.5

[a]In comparison, FR-M has only a 20% larger molecular brightness than FR but is ~2-fold brighter in HeLa cells. These observations suggest that the ~5-fold increase in cellular brightness of FR-MQV relative to FR is due to the combination of an increase in molecular brightness and the increased cellular expression possibly from the L175M substitution.

compared to FR mutants. Thus, cellular imaging studies indicate that FR-MQV retains the high-fidelity localization properties of FR without compromising low cytotoxicity and appropriate maturation and expression.

DISCUSSION

In this work, we engineered FR using a structure-guided approach, aimed to develop mutants with increased fluorescence lifetime manifesting in higher quantum yield, eventually leading to a FP with higher molecular and cellular brightness. We examined both the para-hydroxyphenyl and the acylimine sites of the chromophore for sites where we could potentially increase steric effects, increase rigidity, and interact chemically or electrostatically with the chromophore. This approach led us to mutate multiple residues near the para-hydroxyphenyl moiety, thus motivating the need for lifetime screening of a 7000-member library. In contrast, near the acylimine moiety we identified the capacity for an interaction to be added at position M42. Crystal structure data suggest conformational freedom of the side chain at position 42 in FR.[49] The position 42 lies in close proximity to the acylimine moiety of the chromophore and, based on our previous work, is critical to the hydrogen-bond network on that end of the chromophore in closely related FPs mKate and TagRFP-675.[38,39] A smaller site-saturated library of 20 possible mutants at position 42 allowed us to carry out a plate-based screen on FR-M, where Gln stood out as the best possible side chain residue in terms of increases in fluorescence lifetime and quantum yield.

Individually, L175M, C159V, and M42Q substitutions increased the fluorescence lifetime of FR by ~0.3 ns (~17% increase) and, when incorporated together in FR-MQV, exhibited a ~1 ns (~55%) increase over FR, suggesting that the effect of each mutation in terms of fluorescence lifetime was additive in the triple mutant. FR-MQV closely follows the spectral characteristics of FR-Q and FR-MQ, all of which have reduced spectral widths in absorbance and emission spectra with blue shifts in the absorption spectra with ~20% higher peak absorbance with respect to FR. Consistent with the Strickler−Berg relationship, we calculate higher rate constants for radiative decay in FR mutants with the M42Q mutation. Based on these values, we successfully engineered the decrease of k_{nonrad} with a simultaneous increase of k_{rad} in FR, which is an efficient way of engineering the molecular brightness of a FP. FR-MQV has a k_{rad} comparable to the brightest RFP to date—mScarlet and its cellularly brighter mutant mScarlet-I. Finally, these mutations translate to high cellular brightness without compromising the cellular properties of the parent FR, as seen from the cytotoxicity, maturation, and imaging assays performed in this study. Given this favorable combination of incremental photophysical changes and preserved cellular properties of FR-MQV with respect to FR, further rounds of engineering could produce a new standard for red fluorescent protein labeling.

Crystal structures indicate that the para-hydroxyphenyl moiety of FP chromophores can adopt either the trans (nonfluorescing) or the cis (fluorescing) conformation,[50,51] and in FR, the latter can potentially form a hydrogen bond with the hydroxy group of the S144 residue (Figure 2).[49] The location of C159 suggests that it may play a similar role for the trans conformer of the chromophore. The position 159 was recently discussed to be critical in terms of molecular brightness for FR.[49] The propensity to switch to the trans conformer may be reduced when the residue at this position is substituted for an aliphatic group. The cis to trans isomerization is a reversible process and is manifested as the reversible component of photobleaching under continuous and pulsed (ms to s) illumination.[43,44] The reduction in dark state conversion in the photobleaching kinetics of FR-C159V and FR-C159L indicates that there is a reduction in the tendency of the chromophore to switch to a dark, trans conformer. Furthermore, FR-C159V did not show photoactivation of fluorescence,[52] which suggests that the chromophore might be locked into a single conformation. Leu has a larger aliphatic side chain than Val; thus, the shorter lifetime and complicated photoactivation behavior of FR-C159L may be a steric effect, with Val providing a better spatial fit that restricts chromophore movement into the dark, trans conformer.

Time-resolved ultrafast spectroscopy previously demonstrated that TagRFP-675 and mKate-Q display large Stokes shifts because there are multiple emissive species in the form of non-interconverting hydrogen-bonded conformers.[37−39] Multiple emissive species tend to broaden spectra and correlate with lower quantum yield and shorter fluorescence lifetime values.[38] Steady-state excitation-dependent emission spectra and fluorescence lifetime decay spectra collected in multiple emission windows dismiss the existence of multiple emissive species in M42Q mutants of FR (details in the Supporting Information S4b,j). This is consistent with the minimal change in Stokes shift in the M42Q mutants of FR in comparison to mKate-Q (Supporting Information S4f). The polar side chain of Gln can exist as one of many possible rotamers.[53] It is possible that this residue at position 42 rearranges itself into a conformation that might restrict the number of emissive species. This is supported by UV−vis spectral data. which reveal that incorporating M42Q decreases the spectral width, blue shifts

https://dx.doi.org/10.1021/acs.biochem.0c00484
Biochemistry 2020, 59, 3669−3682

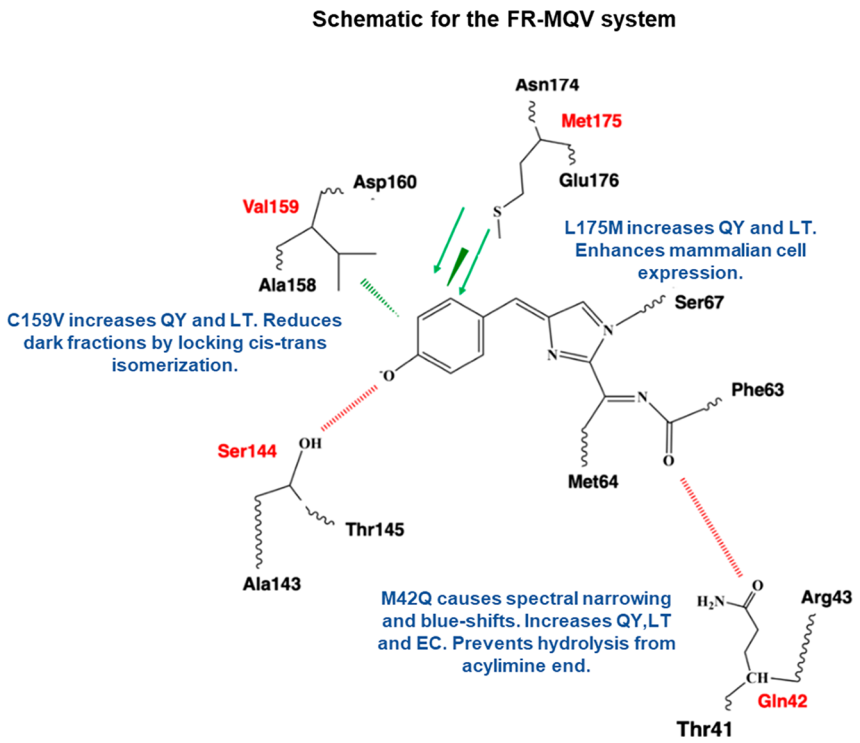

Figure 6. Overall molecular schematic describing the postulated effects of the substitutions in FR-MQV. The L175M mutation increases the quantum yield (QY), fluorescence lifetime (LT), and expression in mammalian cells compared to FR. The C159V mutation reduces the propensity of the cis−trans isomerization of the chromophore and results in subsequent increments in the quantum yield and fluorescence lifetime. The M42Q mutation interacts strongly with the acylimine moiety of the chromophore resulting in blue shifts, spectral narrowing, increased quantum yield, fluorescence lifetime, and extinction coefficient (EC) while also changing in the hydrolysis products of the chromophore.

the absorption and emission spectra, and increases the radiative rate constant. Other than Gln, we observed red fluorescence from the mutant with Ile at this position. Ile is of similar size to Gln and Met but is aliphatic in nature. Characterization of the FR-MI mutant revealed a relative decrease in maximum extinction coefficient and quantum yield with a decrease in fluorescence lifetime with respect to the parent FR-M. We also observed an undesirable green emitting chromophore in the FR-MI and mKate-Q mutants, which was absent from the M42Q mutants of FR (Supporting Information S4i), suggesting complete maturation to a red chromophore in FR-42Q mutants. Alkali denaturation of FR-Q, FR-MQ, and FR-MQV shows cleavage of the chromophore only from the β-carbon of the Tyr side chain, which is indicative of base access to a single site for hydrolysis (Supporting Information S4h). The β-carbon of the Tyr side chain in RFPs is spatially distant (>10 Å based on crystal structure data) from the acylimine moiety of the chromophore. These molecular and photophysical properties suggest that factors other than steric effects (such as electrostatics, hydrogen bonding, etc.) may be responsible for the changes observed in the M42Q mutants of FR.

The ∼5-fold increase in brightness observed in FR-MQV relative to FR (Table 2) is likely an amalgamation of the higher molecular brightness of the M42Q and the C159V mutations along with the higher cellular expression seen for FR-M.[29] The trends for brightness measured through cytometry and microscopy are similar, but FACS measurements employ short laser exposure times with fast, sensitive detectors like photomultiplier tubes (PMTs). In microscopy, cells are subject to relatively longer exposure times and higher irradiances (∼ms time scales) imposed by acquisition times of cameras, which can lead to photobleaching. The correlation between excited-state lifetime and photobleaching (Figure 3f) is evidence that photobleaching occurs due to excited-state absorption, as discussed for other RFPs.[43,54] A practical consequence is that brightness values measured by FACS are systematically higher than those measured in microscopy. This discrepancy between the absolute brightness values between FACS and confocal microscopy measurements was also observed for mScarlet.

Figure 6 is a schematic indicating the postulated effect of each mutation in the development of FR-MQV. Overall, the high extinction coefficient, decrease in the spectral width and blue shifts can be attributed to the M42Q mutation, whereas changes in the dark state behavior with increments in fluorescence lifetime and quantum yield seem to be additive from incorporating the C159V and the L175M mutations into the FR-Q system. All three mutations in FR-MQV face inward, in the vicinity of the chromophore and therefore seem to minimally perturb the cellular properties of FR. The high scores for the OSER and Golgi-localization assays for all FR mutants indicate that cellular properties in FPs are not appreciably affected by mutations of residues with side chains facing toward the chromophore. In the development of FR from mKate and mKate2, most of the mutations that optimized the FP's biological properties were facing out from the β-barrel. We targeted positions to increase brightness, and thus, we did not alter these external positions that were involved in the development of FR from mKate2.[30] Consequently, the mutants retained FR's original performance in terms of localization and cytotoxicity. Though chromophore maturation kinetics can be greatly altered with internal

https://dx.doi.org/10.1021/acs.biochem.0c00484
Biochemistry 2020, 59, 3669−3682

mutations,[28] in this case, chromophore maturation was not substantially slowed by these mutations.

CONCLUSIONS

In this study we present the development of FR-MQV, a FP with high brightness that maintains favorable cellular properties of FR. The C159V mutation appears to play a critical role in restricting the dark state conversion of the protein and increasing fluorescence lifetime, which leads to an increase in quantum yield. The M42Q mutation plays an important role in enhancing the molecular brightness by increasing both the quantum yield and maximum extinction coefficient. Interestingly, this mutation had different effects in closely related FPs including mKate and TagRFP-675. The previously reported L175 M mutation contributes to robust expression levels which improves cellular brightness for FR mutants compared to FR. With its increased brightness and favorable cellular properties, FR-MQV shows promise as a template for further rounds of engineering suited to specific imaging applications like FLIM and FRET. Increasing fluorescence lifetime through further rounds of engineering may increase quantum efficiencies of emission to values near mScarlet with further reduction in the nonradiative rate constant.

ASSOCIATED CONTENT

Supporting Information

The Supporting Information is available free of charge at https://pubs.acs.org/doi/10.1021/acs.biochem.0c00484.

> Additional photophysical characterization, structural/sequence analysis of proteins relevant to the study, and supplemental biochemical/biophysical characterization to support results and data presented in the text (PDF)

Accession Codes

FusionRed (NCBI Accession: 6U1A_A); mKate (NCBI Accession: 3BXB_A); TagRFP-T (NCBI Accession: 5JVA_A); mScarlet (NCBI Accession: APD76535); mCherry (NCBI Accession: ANO45948); EGFP (NCBI Accession: AFA52650); Cytochrome p450- for CytERM-FP tagging (NCBI Accession: KAF4413803.1); and 1,4-galactosyltransferase for GalT-FP tagging (NCBI Accession: AJO20073.1).

AUTHOR INFORMATION

Corresponding Author

Ralph Jimenez − *JILA, University of Colorado at Boulder and National Institute of Standards and Technology, Boulder, Colorado 80309, United States; Department of Chemistry, University of Colorado at Boulder, Boulder, Colorado 80309, United States;* orcid.org/0000-0002-8989-405X; Email: rjimenez@jila.colorado.edu

Authors

Srijit Mukherjee − *JILA, University of Colorado at Boulder and National Institute of Standards and Technology, Boulder, Colorado 80309, United States; Department of Chemistry, University of Colorado at Boulder, Boulder, Colorado 80309, United States*

Sheng-Ting Hung − *JILA, University of Colorado at Boulder and National Institute of Standards and Technology, Boulder, Colorado 80309, United States;* orcid.org/0000-0002-7081-2173

Nancy Douglas − *JILA, University of Colorado at Boulder and National Institute of Standards and Technology, Boulder, Colorado 80309, United States*

Premashis Manna − *Department of Chemistry, MIT, Cambridge, Massachusetts 02139, United States;* orcid.org/0000-0002-6365-6475

Connor Thomas − *JILA, University of Colorado at Boulder and National Institute of Standards and Technology, Boulder, Colorado 80309, United States*

Annika Ekrem − *JILA, University of Colorado at Boulder and National Institute of Standards and Technology, Boulder, Colorado 80309, United States*

Amy E. Palmer − *Department of Biochemistry, University of Colorado at Boulder, Boulder, Colorado 80309, United States; BioFrontiers Institute, University of Colorado, Boulder, Boulder, Colorado 80309, United States;* orcid.org/0000-0002-5794-5983

Complete contact information is available at: https://pubs.acs.org/10.1021/acs.biochem.0c00484

Author Contributions

S.M., S.T.H., P.M., N.D., A.E.P., and R.J. conceived and designed the experiments in the study. S.M., S.T.H., N.D., C.T., A.E., and P.M. performed the experiments. S.M., S.T.H., N.D., A.E.P., and R.J. wrote the manuscript.

Notes

The authors declare no competing financial interest.

ACKNOWLEDGMENTS

S.M. was supported by the NIH/CU Molecular Biophysics Training Program (T32). This work was supported by the NSF Physics Frontier Center at JILA (PHY 1734006 to R.J.) and NIH DP1 GM114863 (to A.E.P.). We thank Dr. Liya Muslinkina at the Macromolecular Crystallography Laboratory of the Frederick National Laboratory for Cancer Research, Argonne, for helpful discussions about the FR crystal structure. We acknowledge Dr. Joe Dragavon, Theresa Nehreini, Dr. Evan Pratt, Dr. Maria Lo, Pia Friis, and David Simpson for their invaluable help with this project. We also express our gratitude towards Shambojit Roy of the Cha-Goodwin Lab at the Chemical and Biological Engineering Department of CU Boulder for the kind gift of chloramphenicol. R.J. is a staff member in the Quantum Physics Division of the National Institute of Standards and Technology (NIST). Certain commercial equipment, instruments, or materials are identified in this paper in order to specify the experimental procedure adequately. Such identification is not intended to imply recommendation or endorsement by the NIST, nor is it intended to imply that the materials or equipment identified are necessarily the best available for the purpose. We acknowledge the Flow Cytometry facility at BioFrontiers Institute, CU Boulder (Grant S10ODO21601). The imaging work was performed at the BioFrontiers Institute Advanced Light Microscopy Core facility. Spinning disc confocal microscopy was performed on a Nikon Ti-E microscope maintained by the BioFrontiers Institute and the Howard Hughes Medical Institute. Spectroscopy was performed at the W.M. Keck Optical Measurements Laboratory in JILA.

REFERENCES

(1) Tsien, R. Y. (1998) The green fluorescent protein. *Annu. Rev. Biochem. 67* (1), 509−544.

(2) Piston, D. W., and Kremers, G. J. (2007) Fluorescent protein FRET: the good, the bad and the ugly. *Trends Biochem. Sci. 32* (9), 407−414.
(3) York, E. M., Weilinger, N. L., LeDue, J. M., and MacVicar, B. A. (2019) Green fluorescent protein emission obscures metabolic fluorescent lifetime imaging of NAD(P)H. *Biomed. Opt. Express 10* (9), 4381−4394.
(4) Levchenko, S. M., Pliss, A., and Qu, J. (2018) Fluorescence lifetime imaging of fluorescent proteins as an effective quantitative tool for noninvasive study of intracellular processes. *J. Innovative Opt. Health Sci. 11* (1), 1730009.
(5) Carter, K. P., Young, A. M., and Palmer, A. E. (2014) Fluorescent sensors for measuring metal ions in living systems. *Chem. Rev. 114* (8), 4564−4601.
(6) Hell, S. W. (2003) Toward fluorescence nanoscopy. *Nat. Biotechnol. 21*, 1347−1355.
(7) Rodriguez, E. A., Tran, G. N., Gross, L. A., Crisp, J. L., Shu, X., Lin, J. Y., and Tsien, R. Y. (2016) A far-red fluorescent protein evolved from a cyanobacterial phycobiliprotein. *Nat. Methods 13*, 763−769.
(8) Shcherbakova, D. M., Baloban, M., Emelyanov, A. V., Brenowitz, M., Guo, P., and Verkhusha, V. V. (2016) Bright monomeric near-infrared fluorescent proteins as tags and biosensors for multiscale imaging. *Nat. Commun. 7*, 12405.
(9) Rainey, K. H., and Patterson, G. H. (2019) Photoswitching FRET to monitor protein−protein interactions. *Proc. Natl. Acad. Sci. U. S. A. 116* (3), 864−873.
(10) Pennacchietti, F., Serebrovskaya, E. O., Faro, A. R., Shemyakina, I. I., Bozhanova, N. G., Kotlobay, A. A., Gurskaya, N. G., Bodén, A., Dreier, J., Chudakov, D. M., Lukyanov, K. A., Verkhusha, V. V., Mishin, A. S., and Testa, I. (2018) Fast reversibly photoswitching red fluorescent proteins for live-cell RESOLFT nanoscopy. *Nat. Methods 15* (8), 601−604.
(11) Cranfill, P. J., Sell, B. R., Baird, M. A., Allen, J. R., Lavagnino, Z., De Gruiter, H. M., Kremers, G. J., Davidson, M. W., Ustione, A., and Piston, D. W. (2016) Quantitative assessment of fluorescent proteins. *Nat. Methods 13* (7), 557−562.
(12) Lambert, T. J. (2019) FPbase: a community-editable fluorescent protein database. *Nat. Methods 16*, 277−278.
(13) Sarkisyan, K. S., Goryashchenko, A. S., Lidsky, P. V., Gorbachev, D. A., Bozhanova, N. G., Gorokhovatsky, A. Y., Pereverzeva, A. R., Ryumina, A. P., Zherdeva, V. V., Savitsky, A. P., Solntsev, K. M., Bommarius, A. S., Sharonov, G. V., Lindquist, J. R., Drobizhev, M., Hughes, T. E., Rebane, A., Lukyanov, K. A., and Mishin, A. S. (2015) Green Fluorescent Protein with Anionic Tryptophan-Based Chromophore and Long Fluorescence Lifetime. *Biophys. J. 109* (2), 380−389.
(14) Goedhart, J., Von Stetten, D., Noirclerc-Savoye, M., Lelimousin, M., Joosen, L., Hink, M. A., Van Weeren, L., Gadella, T. W. J., and Royant, A. (2012) Structure-guided evolution of cyan fluorescent proteins towards a quantum yield of 93%. *Nat. Commun. 3*, 751.
(15) Bindels, D. S., Haarbosch, L., Van Weeren, L., Postma, M., Wiese, K. E., Mastop, M., Aumonier, S., Gotthard, G., Royant, A., Hink, M. A., and Gadella, T. W. J. (2017) mScarlet: A bright monomeric red fluorescent protein for cellular imaging. *Nat. Methods 14* (1), 53−56.
(16) Strickler, S. J., and Berg, R. A. (1962) Relationship between absorption intensity and fluorescence lifetime of molecules. *J. Chem. Phys. 37* (4), 814−822.
(17) Manas, E. S., and Spano, F. C. (1998) Absorption and spontaneous emission in aggregates of conjugated polymers. *J. Chem. Phys. 109* (18), 8087−8101.
(18) Canty, L., Hariharan, S., Liu, Q., Haney, S. A., and Andrews, D. W. (2018) Peak emission wavelength and fluorescence lifetime are coupled in far-red, GFP-like fluorescent proteins. *PLoS One 13* (11), e0208075.
(19) Mamontova, A. V., Solovyev, I. D., Savitsky, A. P., Shakhov, A., Lukyanov, K. A., and Bogdanov, A. M. (2018) Bright GFP with subnanosecond fluorescence lifetime. *Sci. Rep. 8*, 13224.
(20) Piatkevich, K. D., Efremenko, E. N., Verkhusha, V. V., and Varfolomeev, S. D. (2010) Red fluorescent proteins and their properties. *Russ. Chem. Rev. 79* (3), 243−258.
(21) Miyawaki, A., Shcherbakova, D. M., and Verkhusha, V. V. (2012) Red fluorescent proteins: Chromophore formation and cellular applications. *Curr. Opin. Struct. Biol. 22* (5), 679−688.
(22) Subach, F. V., and Verkhusha, V. V. (2012) Chromophore transformations in red fluorescent proteins. *Chem. Rev. 112* (7), 4308−4327.
(23) Prangsma, J. C., Molenaar, R., van Weeren, L., Bindels, D. S., Haarbosch, L., Stouthamer, J., Gadella, T. W. J., Subramaniam, V., Vos, W. L., and Blum, C. (2020) Quantitative Determination of Dark Chromophore Population Explains the Apparent Low Quantum Yield of Red Fluorescent Proteins. *J. Phys. Chem. B 124* (8), 1383−1391.
(24) Dunsing, V., Luckner, M., Zühlke, B., Petazzi, R. A., Herrmann, A., and Chiantia, S. (2018) Optimal fluorescent protein tags for quantifying protein oligomerization in living cells. *Sci. Rep. 8*, 10634.
(25) Moron, V., Marazzi, M., and Wanko, M. (2019) Far Red Fluorescent Proteins: Where Is the Limit of the Acylimine Chromophore? *J. Chem. Theory Comput. 15* (7), 4228−4240.
(26) Park, J. W., and Rhee, Y. M. (2016) Electric Field Keeps Chromophore Planar and Produces High Yield Fluorescence in Green Fluorescent Protein. *J. Am. Chem. Soc. 138* (41), 13619−13629.
(27) Simine, L., Lammert, H., Sun, L., Onuchic, J. N., and Rossky, P. J. (2018) Fluorescent Proteins Detect Host Structural Rearrangements via Electrostatic Mechanism. *J. Am. Chem. Soc. 140* (4), 1203−1206.
(28) Balleza, E., Kim, J. M., and Cluzel, P. (2018) Systematic characterization of maturation time of fluorescent proteins in living cells. *Nat. Methods 15* (1), 47−51.
(29) Manna, P., Hung, S. T., Mukherjee, S., Friis, P., Simpson, D. M., Lo, M. N., Palmer, A. E., and Jimenez, R. (2018) Directed evolution of excited state lifetime and brightness in FusionRed using a microfluidic sorter. *Integrative Biology (United Kingdom) 10* (9), 516−526.
(30) Shemiakina, I. I., Ermakova, G. V., Cranfill, P. J., Baird, M. A., Evans, R. A., Souslova, E. A., Staroverov, D. B., Gorokhovatsky, A. Y., Putintseva, E. V., Gorodnicheva, T. V., Chepurnykh, T. V., Strukova, L., Lukyanov, S., Zaraisky, A. G., Davidson, M. W., Chudakov, D. M., and Shcherbo, D. (2012) A monomeric red fluorescent protein with low cytotoxicity. *Nat. Commun. 3*, 1204.
(31) Hung, S. T., Mukherjee, S., and Jimenez, R. (2020) Enrichment of rare events using a multi-parameter high throughput microfluidic droplet sorter. *Lab Chip 20* (4), 834−843.
(32) Kamentsky, L., Jones, T. R., Fraser, A., Bray, M. A., Logan, D. J., Madden, K. L., Ljosa, V., Rueden, C., Eliceiri, K. W., and Carpenter, A. E. (2011) Improved structure, function and compatibility for cellprofiler: Modular high-throughput image analysis software. *Bioinformatics 27* (8), 1179−1180.
(33) Schindelin, J., Arganda-Carreras, I., Frise, E., Kaynig, V., Longair, M., Pietzsch, T., Preibisch, S., Rueden, C., Saalfeld, S., Schmid, B., Tinevez, J. Y., White, D. J., Hartenstein, V., Eliceiri, K., Tomancak, P., and Cardona, A. (2012) Fiji: An open-source platform for biological-image analysis. *Nat. Methods 9*, 676−682.
(34) Ansari, A. M., Ahmed, A. K., Matsangos, A. E., Lay, F., Born, L. J., Marti, G., Harmon, J. W., and Sun, Z. (2016) Cellular GFP Toxicity and Immunogenicity: Potential Confounders in in Vivo Cell Tracking Experiments. *Stem Cell Reviews and Reports 12* (5), 553−559.
(35) Liu, B., Mavrova, S. N., Van Den Berg, J., Kristensen, S. K., Mantovanelli, L., Veenhoff, L. M., Poolman, B., and Boersma, A. J. (2018) Influence of Fluorescent Protein Maturation on FRET Measurements in Living Cells. *ACS Sensors 3* (9), 1735−1742.
(36) Piatkevich, K. D., Malashkevich, V. N., Morozova, K. S., Nemkovich, N. A., Almo, S. C., and Verkhusha, V. V. (2013)

https://dx.doi.org/10.1021/acs.biochem.0c00484
Biochemistry 2020, 59, 3669−3682

Extended stokes shift in fluorescent proteins: Chromophore-protein interactions in a near-infrared TagRFP675 variant. *Sci. Rep.* 3, 1847.
(37) Yoon, E., Konold, P. E., Lee, J., Joo, T., and Jimenez, R. (2016) Far-Red Emission of mPlum Fluorescent Protein Results from Excited-State Interconversion between Chromophore Hydrogen-Bonding States. *J. Phys. Chem. Lett.* 7 (12), 2170−2174.
(38) Konold, P., Regmi, C. K., Chapagain, P. P., Gerstman, B. S., and Jimenez, R. (2014) Hydrogen bond flexibility correlates with stokes shift in mPlum variants. *J. Phys. Chem. B 118* (11), 2940−2948.
(39) Konold, P. E., Yoon, E., Lee, J., Allen, S. L., Chapagain, P. P., Gerstman, B. S., Regmi, C. K., Piatkevich, K. D., Verkhusha, V. V., Joo, T., and Jimenez, R. (2016) Fluorescence from Multiple Chromophore Hydrogen-Bonding States in the Far-Red Protein TagRFP675. *J. Phys. Chem. Lett.* 7 (15), 3046−3051.
(40) DeLano, W. L. *The PyMOL Molecular Graphics System, Version 1.1*, Schrödinger LLC.
(41) Martynov, V. I., Savitsky, A. P., Martynova, N. Y., Savitsky, P. A., Lukyanov, K. A., and Lukyanov, S. A. (2001) Alternative cyclization in GFP-like proteins family. The formation and structure of the chromophore of a purple chromoprotein from Anemonia sulcata. *J. Biol. Chem. 276* (24), 21012−21016.
(42) Tretyakova, Y. A., Pakhomov, A. A., and Martynov, V. I. (2007) Chromophore structure of the kindling fluorescent protein asFP595 from Anemonia sulcata. *J. Am. Chem. Soc. 129* (25), 7748−7749.
(43) Dean, K. M., Lubbeck, J. L., Binder, J. K., Schwall, L. R., Jimenez, R., and Palmer, A. E. (2011) Analysis of red-fluorescent proteins provides insight into dark-state conversion and photodegradation. *Biophys. J. 101* (4), 961−969.
(44) Manna, P., and Jimenez, R. (2015) Time and frequency-domain measurement of ground-state recovery times in red fluorescent proteins. *J. Phys. Chem. B 119* (15), 4944−4964.
(45) Kruitwagen, T., Denoth-Lippuner, A., Wilkins, B. J., Neumann, H., and Barral, Y. (2015) Axial contraction and short-range compaction of chromatin synergistically promote mitotic chromosome condensation. *eLife 4*, e10396.
(46) Kimura, S., Noda, T., and Yoshimori, T. (2007) Dissection of the autophagosome maturation process by a novel reporter protein, tandem fluorescent tagged LC3. *Autophagy 3* (5), 452−460.
(47) Costantini, L. M., Fossati, M., Francolini, M., and Snapp, E. L. (2012) Assessing the Tendency of Fluorescent Proteins to Oligomerize Under Physiologic Conditions. *Traffic 13* (5), 643−649.
(48) Costantini, L. M., Baloban, M., Markwardt, M. L., Rizzo, M., Guo, F., Verkhusha, V. V., and Snapp, E. L. (2015) A palette of fluorescent proteins optimized for diverse cellular environments. *Nat. Commun. 6*, 7670.
(49) Muslinkina, L., Pletnev, V. Z., Pletneva, N. V., Ruchkin, D. A., Kolesov, D. V., Bogdanov, A. M., Kost, L., Rakitina, T. V., Agapova, Yu. K., Shemyakina, I. I., Chudakov, D. M., and Pletnev, S. (2020) Two Independent Routes of Post-Translational Chemistry in Fluorescent Protein FusionRed. *Int. J. Biol. Macromol. 155*, 551−559.
(50) Pletneva, N. V., Pletnev, V. Z., Shemiakina, I. I., Chudakov, D. M., Artemyev, I., Wlodawer, A., Dauter, Z., and Pletnev, S. (2011) Crystallographic study of red fluorescent protein eqFP578 and its far-red variant Katushka reveals opposite pH-induced isomerization of chromophore. *Protein Sci. 20* (7), 1265−1274.
(51) Zhou, X. X., and Lin, M. Z. (2013) Photoswitchable fluorescent proteins: Ten years of colorful chemistry and exciting applications. *Curr. Opin. Chem. Biol. 17* (4), 682−690.
(52) Stiel, A. C., Andresen, M., Bock, H., Hilbert, M., Schilde, J., Schönle, A., Eggeling, C., Egner, A., Hell, S. W., and Jakobs, S. (2008) Generation of monomeric reversibly switchable red fluorescent proteins for far field fluorescence nanoscopy. *Biophys. J. 95* (6), 2989−2997.
(53) Lovell, S. C., Word, J. M., Richardson, J. S., and Richardson, D. C. (1999) Asparagine and glutamine rotamers: B-factor cutoff and correction of amide flips yield distinct clustering. *Proc. Natl. Acad. Sci. U. S. A. 96* (2), 400−405.
(54) Dean, K. M., Lubbeck, J. L., Davis, L. M., Regmi, C. K., Chapagain, P. P., Gerstman, B. S., Jimenez, R., and Palmer, A. E. (2015) Microfluidics-based selection of red-fluorescent proteins with decreased rates of photobleaching. *Integrative Biology (United Kingdom) 7* (2), 263−73.

https://dx.doi.org/10.1021/acs.biochem.0c00484
Biochemistry 2020, 59, 3669−3682